Palaeogeography, Palaeoclimatology, Palaeoecology 584 (2021) 110681

Contents lists available at ScienceDirect

Palaeogeography, Palaeoclimatology, Palaeoecology

journal homepage: www.elsevier.com/locate/palaeo

Invited Research Article

The Messinian evaporites of the Mesaoria basin (North Cyprus): A discrepancy with the current chronostratigraphic understanding

D. Artiaga [a], J. García-Veigas [a,*], D.I. Cendón [b], C. Atalar [c], L. Gibert [d]

[a] Scientific and Technological Centers, University of Barcelona (CCiTUB), 08028 Barcelona, Spain
[b] Australian Nuclear Science and Technology Organization (ANSTO), Kirrawee DC, NSW 2052, Australia
[c] Department of Civil Engineering, Near East University, Lefkosa, Cyprus
[d] Department of Mineralogy, Petrology and Applied Geology, University of Barcelona, 08028 Barcelona, Spain

ARTICLE INFO

Editor: A. Dickson

Keywords:
Messinian
Sulfur isotopes
Oxygen (in sulfate) isotopes
Strontium isotopes
Evaporites
Gypsum deposits
Cyprus

ABSTRACT

Large volume of evaporites were deposited during the Messinian Salinity Crisis (MSC) across the Mediterranean. These evaporites are currently outcropping on land and are interpreted by seismic profiles beneath the Mediterranean floor. Biostratigraphic, magnetostratigraphic and astrochronologic data recovered from sediments below and above outcropping evaporites, together with gypsum facies associations and stratigraphic cyclicity, are the cornerstone of what is known as the MSC 'three-stage' model: Primary Lower Gypsum (PLG) – MSC stage 1, Resedimented Lower Gypsum (RLG) - MSC stage 2, and Upper Gypsum (UG) – MSC stage 3. Although this litho- and chronostratigraphic model is mainly based on the gypsum succession in Sicily, it is being currently applied by many investigators across the Mediterranean.

The Mesaoria basin, in North Cyprus, hosts well exposed MSC gypsum deposits of the Kalavasos Fm. Two informal units are distinguished in the gypsum succession. The lower unit, largely consisting of clastic gypsum deposits, is conformably overlaid by the upper unit, mostly consisting of 'in situ' vertically-oriented selenite deposits. Based on the lithostratigraphic gypsum succession, the lower unit could be tentatively assigned to RLG - MSC stage 2, while the upper unit could correspond to UG - MSC stage 3. However, our lithologic and geochemical ($\delta^{34}S_{sulfate}$ $\delta^{18}O_{sulfate}$, $^{87}Sr/^{86}Sr$) data in gypsum points that the upper unit fits with those of the PLG – MSC stage 1.

For the first time, thick vertically-oriented selenite beds with lithofacies and geochemical signatures diagnostic of PLG deposits lay conformably over clastic gypsum successions diagnostic of RLG deposits in the currently accepted 'three-stage' model. In North Cyprus, 'in situ' selenite platforms and 'clastic' gravity-flow gypsum deposits are coeval involving erosion and redeposition during the same evolutive stage.

The complete gypsum succession in North Cyprus must be considered as MSC Lower Evaporites in the 'two-step' model (Lower Evaporites and Upper Evaporites) classically proposed prior to the 'three-stage' model.

We show how nearby Messinian evaporite basins in the same island (North and South Cyprus) can produce different sedimentary records. Our data cast doubts on the systematic application of the 'three-stage' litho- and chronostratigraphic model to North Cyprus and other MSC Mediterranean evaporite successions.

This work highlights the importance of local processes in the sedimentation and distribution of MSC evaporites in active tectonic settings, and alerts against extrabasinal MSC correlations based on gypsum facies distribution.

1. Introduction

1.1. The Messinian Salinity Crisis

The Messinian Salinity Crisis (MSC) represents the most dramatic environmental change in the Mediterranean basin over the Neogene. The restriction of the exchanges between the Atlantic and the Mediterranean, triggered by tectonic variations and potentially amplified by climate shifts, lead to a significant change in the marine sedimentation of the Mediterranean. This caused the deposition of a great volume of

* Corresponding author.
E-mail addresses: dartiaga@ub.edu (D. Artiaga), garcia_veigas@ub.edu (J. García-Veigas), dce@ansto.gov.au (D.I. Cendón), cavit.atalar@neu.edu.tr (C. Atalar), lgibert@ub.edu (L. Gibert).

https://doi.org/10.1016/j.palaeo.2021.110681
Received 11 June 2021; Received in revised form 22 September 2021; Accepted 27 September 2021
Available online 4 October 2021

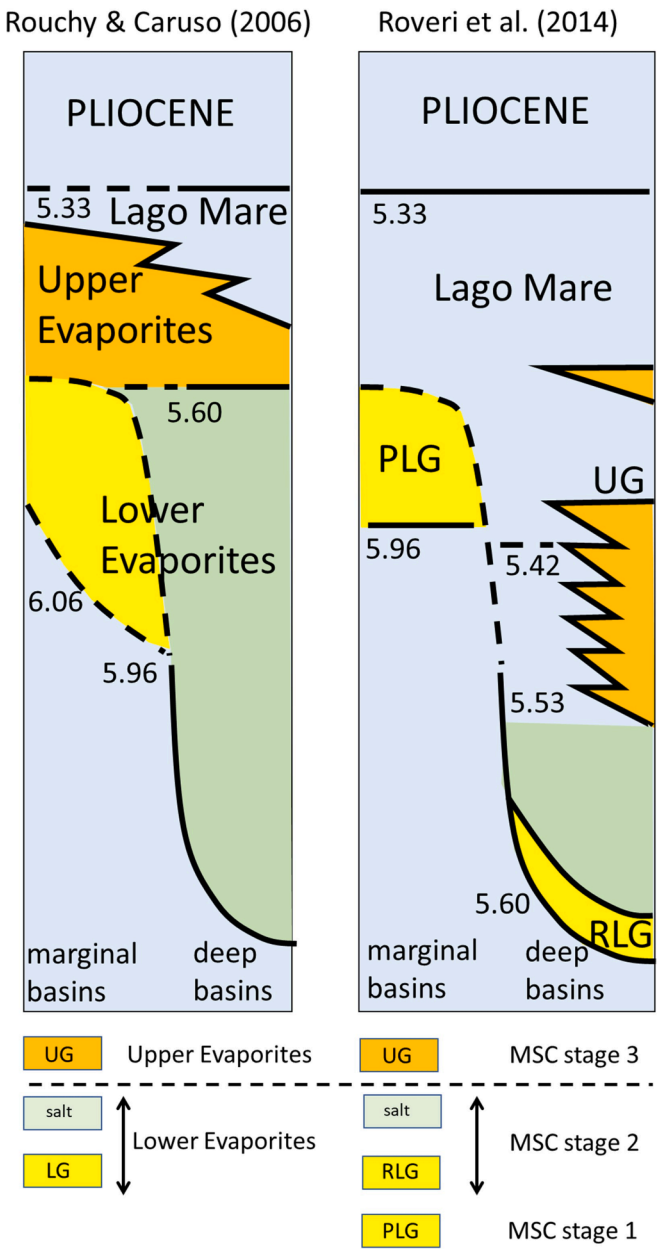

Fig. 1. Evaporite units and nomenclature equivalence between the MSC litho- and chronostratigraphic frameworks proposed by Rouchy and Caruso (2006) and by Roveri et al. (2014a).

evaporites in marginal, intermediate-deep and deep Mediterranean basins (Ogniben, 1957; Selly, 1973; Hsü et al., 1973; Ryan, 1976; Clauzon et al., 1996; Krijgsman et al., 1999; Manzi et al., 2013). Over decades, geoscientists have pursued the development of a comprehensive model that would facilitate stratigraphic correlations across the Mediterranean basin (summarized in Rouchy and Caruso, 2006, and Roveri et al., 2014a). However, difficulties have been compounded by the inclusion of the complete MSC event within a sole reversed magnetic chron, absence of precise radiometric ages and shortcomings of biostratigraphic markers. These combined have made difficult to establish stratigraphic and genetic correlations between evaporites formed in marginal and deeper offshore basins.

Based on seismic borehole data and comparison between mostly Sicilian Messinian evaporite successions, a 'two-step' informal division into Lower Evaporites (Lower Gypsum and Halite Unit) and Upper Evaporites (Upper Gypsum) was originally proposed for MSC Mediterranean evaporite deposits (Hsü et al., 1973; Hsü et al., 1977; Cita et al., 1978; Rouchy, 1982; Müller and Mueller, 1991; Butler et al., 1995; Clauzon et al., 1996; Krijgsman et al., 1999; Rouchy and Caruso, 2006).

More recently, Roveri et al. (2014a) readapting previous proposals (CIESM, 2008; Roveri et al., 2008b; Manzi et al., 2013) suggest a new litho- and chronostratigraphic division of the MSC into three evolutionary stages (Fig. 1). In the three-stage model (Roveri et al., 2014a), the MSC stage 1 (5.96–5.60 Ma) is characterized by primary 'in situ' vertically-oriented selenite deposits (Primary Lower Gypsum – PLG) formed in relatively shallow silled basins (Roveri et al., 2008b; Lugli et al., 2010). During the second stage (5.60–5.53 Ma), an intense reduction of the Atlantic-Mediterranean exchange led to a Mediterranean sea-level drop. This fall caused an extensive subaerial erosion of the Mediterranean margins expressed in most of the marginal and intermediate deep basins in the form of a prominent erosional surface (Messinian Erosional Surface – MES) and on clastic gypsum deposits derived from the resedimentation of PLG deposits (Resedimented Lower Gypsum – RLG). In combination with the erosion of the margins, halite is though to have accumulated in the deepest basins (Clauzon et al., 1996; Lofi et al., 2005; Roveri et al., 2008b). The third stage (5.53–5.33 Ma) is characterized by a twofold sedimentary expression (see Andreetto et al., 2021, for a comprehensive review): terrigenous deposits and minor carbonates containing Lago Mare biofacies in the shallower basins, a mixing of in-situ Paratethyan biota indicative of fresh to brackish water conditions and marine biota of doubtful provenance (e.g. Fortuin, 2003; Rouchy et al., 2007; Guerra-Merchán et al., 2014), and by selenite gypsum and fine-grained cumulated gypsum (balatino) deposits alternating with marls (Upper Gypsum – UG) (Manzi et al., 2009).

The Lower Evaporites in the classical MSC division (Rouchy and Caruso, 2006, for a review) include the PLG (MSC stage 1) and the RLG (MSC stage 2) deposits, differentiated in the Roveri et al. (2014a) model (Fig. 1). Gypsum successions considered as Upper Evaporites in the classical model are equivalent to UG (MSC stage 3) deposits in the Roveri et al. (2014a) model.

In Cyprus, due to recent historical constraints, most of the MSC work has been carried out in South Cyprus (Polemi, Psemastimenos and Pissouri basins) (Fig. 2). However, Messinian evaporites crop out extensively in the Mesaoria basin, in North Cyprus (Fig. 2) (Gass, 1960; Gass and Cockbain, 1961; Necdet and Anıl, 2006; Varol and Atalar, 2017).

Based on bio- and magnetostratigraphic data, the onset of the MSC in South Cyprus has been placed within the pre-evaporitic Pakhna Fm. (Krijgsman et al., 2002; Orszag-Sperber et al., 2009), or in the contact between the Pakhna and the Kalavasos Fm. (Manzi et al., 2016). According to Manzi et al. (2016), in South Cyprus, the Kalavasos Fm. contains gypsum deposits of the second (RLG) and the third (UG) stages defined in the Roveri et al. (2014a) model. Unlike in southern counterparts, there are no biostratigraphic or magnetostratigraphic published data to support any chronostratographic assignation for the MSC onset in North Cyprus.

Variations of sulfur and oxygen (in sulfate) isotope compositions ($\delta^{34}S_{sulfate}$ and $\delta^{18}O_{sulfate}$) and $^{87}Sr/^{86}Sr$ ratios in evaporite sedimentary deposits are an important tool to differentiate sources and processes of brines. To this present study, sulfate and strontium isotope data of the North Cyprus evaporites was limited to a gypsum quarry (Kato Moni) in the southern margin of the Mesaoria basin. Based on $\delta^{34}S_{sulfate}$ and $\delta^{18}O_{sulfate}$, Pierre (1982) assign the Kato Moni gypsum to Lower Evaporites in the classical MSC division. Subsequently, Manzi et al. (2016), based on gypsum lithofacies, reassign the Kato Moni gypsum to the UG unit (MSC stage 3) in the Roveri et al. (2014a) model.

In this study, we present the first systematic lithostratigraphic, petrographic, and geochemical study of different MSC evaporite sections in the southern and northern margins of the Mesaoria basin (North Cyprus). The aims of this paper are: 1) to propose a sedimentological model for the MSC gypsum deposits in the Mesaoria basin; 2) to establish a stratigraphic correlation chart between different outcropped sections; 3) to compare the isotope signatures of the North Cyprus evaporites with

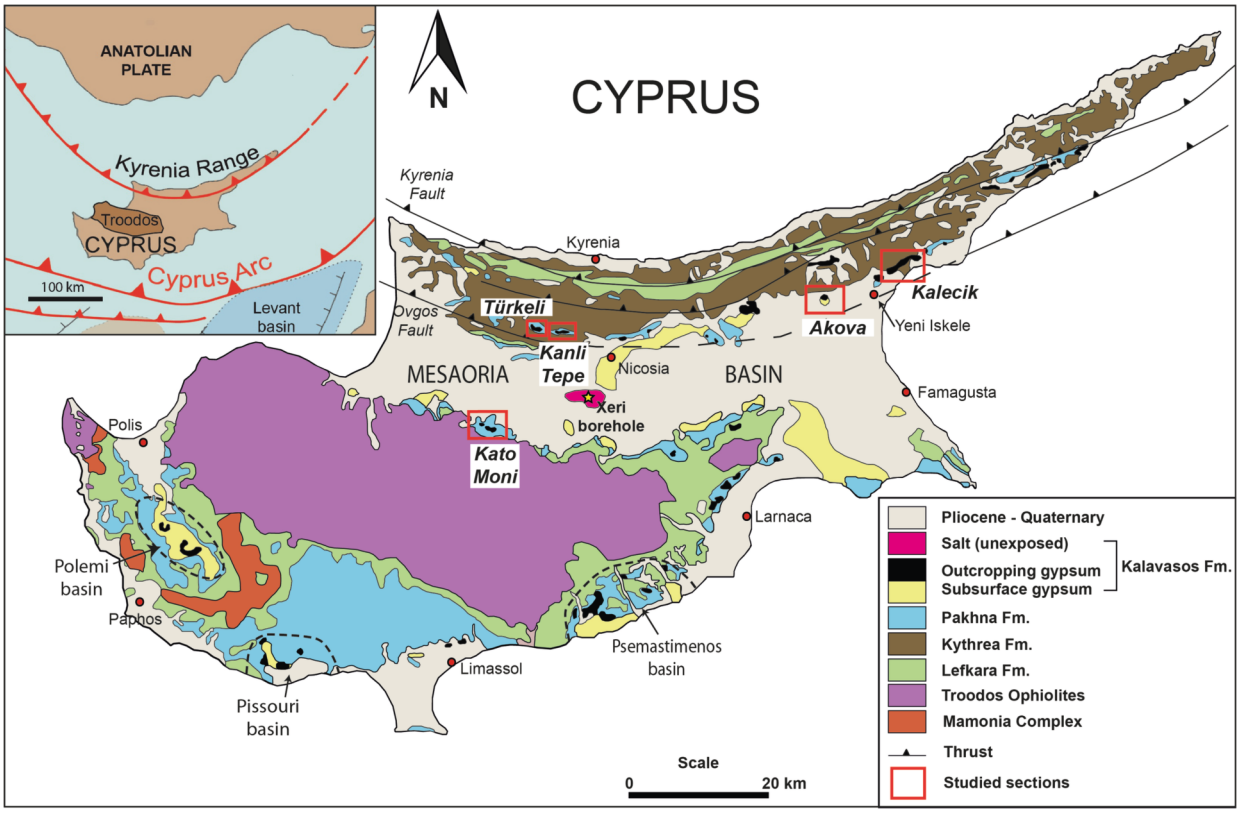

Fig. 2. Geologic map of Cyprus (modified from Pantazis, 1976). Location of the studied MSC gypsum successions in the Mesaoria basin (North Cyprus).

those reported for other MSC deposits; and 4) to discuss the integration of the North Cyprus evaporites within the Roveri et al. (2014a) stratigraphic framework proposed for the MSC.

1.2. Chemostratigraphy of the MSC evaporites

The ocean sulfate concentration and its isotopic composition have varied over geological time scales. Isotope compositions of $\delta^{34}S \sim 22‰$ and $\delta^{18}O \sim 12‰$ are expected for sulfate minerals precipitated from evaporated Late Miocene seawater (Claypool et al., 1980; Kasprzyk, 1997; Paytan et al., 1998; Turchyn and Schrag, 2004; Kampschulte and Strauss, 2004).

In MSC western and central Mediterranean evaporites, sulfate isotope compositions of $\delta^{34}S \sim 23‰$ and $\delta^{18}O \sim 14‰$ are reported for Lower Evaporites (PLG and RLG deposits) in Sorbas, Bajo Segura, Mallorca, Níjar (Spain), in Caltanissetta (Sicily) and in Polemi (South Cyprus) basins (Pierre, 1982; Lu et al., 2001; Lu and Meyers, 2003; García-Veigas et al., 2018). These values are higher ($\sim 1‰$ in $\delta^{34}S$, $\sim 2‰$ in $\delta^{18}O$) than those expected for Late Miocene marine evaporites.

Reported $\delta^{34}S_{sulfate}$ and $\delta^{18}O_{sulfate}$ data for Upper Evaporites (UG, MSC stage 3) successions are sparse, with values of ~23‰ for $\delta^{34}S$ and ~ 17‰ for $\delta^{18}O$ in Sicily (García-Veigas et al., 2018), and of ~23‰ and ~ 19‰ respectively in South Cyprus (Pierre, 1982). According to these data, the Upper Evaporites show enrichments of ~1‰ for $\delta^{34}S$, and of 5–7‰ for $\delta^{18}O$, with respect to values expected for Late Miocene marine evaporites.

Although similar $\delta^{34}S$ values (~ 23‰) characterize all MSC gypsum deposits, marked differences in $\delta^{18}O$ permit distinguishing between Lower Evaporites - PLG and RLG units (~ 14‰), and Upper Evaporites – UG units (~ 17–19‰).

Strontium isotope ratios ($^{87}Sr/^{86}Sr$) in sedimentary gypsums preserve the isotopic signature of the water source where they precipitated. $^{87}Sr/^{86}Sr$ in well-mixed ocean waters is homogeneous. The oceanic strontium ratio has changed over geological times as consequence of the balance between different Sr sources (Palmer and Edmond, 1992; Reinhardt et al., 1998; Krabbenhöft et al., 2010; Pearce et al., 2015).

$^{87}Sr/^{86}Sr$ variations follow a particular trend throughout the MSC deposits. This trend shows a gradual and rapid detachment from the global ocean line (Flecker et al., 2002; Flecker and Ellam, 2006; Topper et al., 2011; Roveri et al., 2014b; García-Veigas et al., 2018). Strontium isotope ratios in Lower Evaporites (PLG and RLG units) are in range, or close, to the global ocean line ($^{87}Sr/^{86}Sr$: 0.7089–0.7090). Upper Evaporites (UG units) show a marked fall in Sr isotope ratios (0.7087–0.7088) interpreted as linked to the progressive closure of Mediterranean gateways and the increase of freshwater inputs (Flecker et al., 2002; Flecker and Ellam, 2006).

Although sulfate and strontium isotopic signatures in gypsum can be used as good indicators for chemostratigraphic correlations in intermediate and deep basins, mainly fed by marine inputs, the extension towards more marginal basins, with major continental inputs, could be questionable if geochemical end-members are not well constrained. This is the case of the gypsum succession in the Maiella section (Central Apennines), assigned to MSC Lower Evaporites (Sampalmieri et al., 2008; Samplamieri et al., 2010) but reporting some $^{87}Sr/^{86}Sr$ values in disagreement with those obtained in most of the MSC Lower Evaporites (Roveri et al., 2014b, and references therein).

1.3. Geological setting

The Eastern Mediterranean region consists of several small Neotethyan oceanic basins created and destroyed in a complex geodynamic framework between the African, Arabian and Eurasian lithospheric plates and the smaller Anatolian microplate (Fig. 2) (Kinnaird, 2008; McCay, 2011; Papadimitriou et al., 2018). The island of Cyprus, located in the easternmost part of the Mediterranean region, was formed by the collision and stacking of three main tectonic terranes: the northerly Kyrenia Range, a fragment detached from the southern margin of Anatolian microplate; the central Troodos Ophiolitic Massif; and the

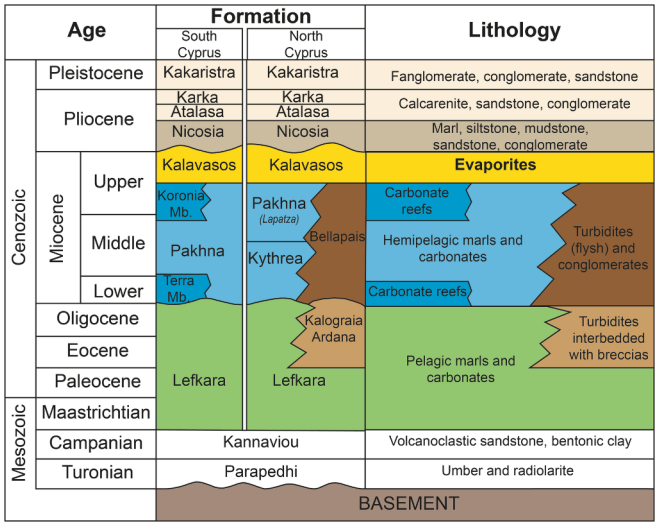

Fig. 3. Mesozoic to Pleistocene lithostratigraphic units of Cyprus (modified from Roberston et al., 1995).

southerly Mamonia Complex, a fragment of the continental margin of the African plate (Kinnaird and Robertson, 2012; Papadimitriou et al., 2018). These tectonic terranes form the basement on which several Cenozoic sedimentary basins formed.

The Mesaoria basin is a tectonically active basin, bounded to the north by the Kyrenia Range and to the south by the Troodos Ophiolitic Massif (Fig. 2). The depositional settings of the basin were strongly influenced by the regional tectonic activity (Robertson and Kinnaird, 2016). From the Late Cretaceous (Maastrichtian) to the Oligocene, the island of Cyprus was a deep marine setting where pelagic marls and carbonates (Lefkara Fm.) deposited (Fig. 3) (Robertson and Hudson, 1974; Robertson et al., 1995; Kinnaird et al., 2011). During the Late Eocene, a regional southward thrusting related to the subduction of the northern Troodos oceanic crust beneath the Anatolian microplate (Kyrenia range) resulted in the deposition of debris flows in the foredeep domain (Kalograia-Ardana Fm. – Lapithos Group) (Fig. 3).

The structural evolution of North Cyprus from the Late Eocene to recent times is still unclear. Recent tectonic reconstructions (Kinnaird, 2008; Kinnaird and Robertson, 2012; Robertson and Kinnaird, 2016; Robertson et al., 2019) suggest that northward subduction to the south of Cyprus initiated in the Late Oligocene - Early Miocene causing the uplift of the Troodos Ophiolitic Massif and a progressive shallowing with deposition of the hemipelagic marine carbonates and carbonate reefs of the Pakhna Fm. (Fig. 3) (Kinnaird et al., 2011).

A second convergence phase, during the Middle - Late Miocene, resulted in the Kyrenia thrust belt dock. As a result of the on-going convergence, the foredeep domain between the Kyrenia Range and the Troodos Massif was segmented into two depocenters (Robertson et al., 2019). Fine-grained terrigenous turbidites (Bellapais Fm. – Kythrea Group) (Fig. 3) deposited in the vicinities of the Kyrenia Range. The convergence phase continued during Late Miocene (Messinian) - Early Pliocene (McCay and Robertson, 2013; Robertson and Kinnaird, 2016) resulting in a high subsidence of the Mesaoria basin. The tectonic configuration of the basin, and the progressive restriction of the Atlantic-Mediterrean connection, led to deposition of the Messinian evaporites (Kalavasos Fm.) (Fig. 3), consisting of up to 100 m thick outcropping gypsum deposits, and a salt unit (~ 300 m thick) identified by borehole and seismic profiles in the subsurface of the Mesaoria plain (Gass, 1960; Zomenis, 1972). The Early Pliocene was characterized by a quiescent tectonic period as well as by a transgressive trend causing the deposition of the Nicosia Fm. pelagic sediments (Fig. 3) (Palamakumbura and Robertson, 2016).

2. Material and methods

This study concentrates on different gypsum successions outcropping in both the southern and northern margins of the Mesaoria basin in North Cyprus (Fig. 2).

More than 50 hand samples and thin sections of gypsum have been studied with petrographic and scanning electron microscopes (SEM-EDS). Several chips of the fine-grained gypsum and of different selenite crystals were selected for SEM-EDS observations and isotopic determinations.

SEM observations have been performed at the Scientific and Technological Centers of the University of Barcelona (CCiTUB) with a FEI Quanta-200 and a Jeol-7100F Field Emission SEM, both equipped with energy dispersive X-Ray spectrometers for elemental identifications (EDS).

Sulfur and oxygen isotope compositions ($\delta^{34}S_{sulfate}$ and $\delta^{18}O_{sulfate}$) in gypsum samples ($n = 30$) have been determined at the CCiTUB. Gypsum samples were dissolved in ultrapure water, filtered to remove insoluble material and acidified to pH 3 to eliminate carbonates. Dissolved sulfate was reprecipitated as $BaSO_4$ by addition of a $BaCl_2$ solution. Isotope determinations were performed with an ISOGAS Sira-9 Spectrometer and a Thermo Finnigan Delta Plus XP Spectrometer. The analytical error (2σ) is ±0.3‰ for $\delta^{34}S$ and $\delta^{18}O$. Values obtained for the international standard NBS-127 are $\delta^{34}S$: 20.3 ± 0.1‰ and $\delta^{18}O$: 9.3 ± 0.2‰.

The $^{87}Sr/^{86}Sr$ in gypsum samples have been measured at the University of Queensland, Australia. Dissolved samples in 2 N HNO_3 were loaded onto columns pre-filled with 0.19 ml of Eichrom Sr-spec resin (50–100 μm). The Sr was released from the columns and collected using 2.8 ml 0.05 N HNO_3. The Sr concentrations were then screened on a Thermo X-series II quadrupole Inductively Couple Plasma Mass Spectrometer (ICP-MS). Based on the screened results, a 3 ml dilute aliquot in 2% HNO_3 (vol/vol) was made for each sample for measurement of Sr isotopic compositions on a Nu Plasma HR Multi-collector ICP-MS. Mass fractionation were corrected by normalizing the raw ratios to $^{86}Sr/^{88}Sr = 0.1196$. Repeated measurements of a SRM-987 standard solution of a similar concentration to the samples was measured every five samples giving $^{87}Sr/^{86}Sr$ ratios of 0.710249 ± 0.000006 (2σ, $n = 4$).

3. Results

3.1. Gypsum lithofacies in the Mesaoria basin

In North Cyprus, the MSC evaporites of the Mesaoria basin crop out in the northern margin along a 150 km^2 E – W area in up to 22 gypsum quarries (Necdet and Anıl, 2006; Varol and Atalar, 2017). However, only few, gypsum successions crop out in the southern margin of the basin, close to the Troodos Ophiolitic Massif (Fig. 2).

Gypsum in North Cyprus MSC deposits can be grouped into three main groups of lithofacies: 1) fine-grained laminated gypsum, 2) vertically-oriented selenites, which include massive and banded selenite facies (Babel, 2007, Lugli et al., 2010) and selenite clusters, and 3) clastic gypsum, including gypsarenites and gypsirudites. Fine-grained laminated gypsum lithofacies, labeled “Marmara” in Cyprus, have been considered by Robertson et al. (1995) and Roveri and Manzi (2006) equivalent to the “Balatino” term used in Italy. The Marmara gypsum consists of fine-laminated gypsum formed by alternating darker and lighter laminae (mm - cm size). The darker laminae are composed by gypsum crystals mixed with micritic carbonate (mostly dolomite), while lighter laminae are mainly formed by gypsum. Under the microscope gypsum laminae are made up of two different gypsum microfacies. The most common microfacies consist of prismatic equant gypsum crystals (50–200 μm size) showing blocky texture, the other consist of acicular gypsum crystals (< 0.5 mm long) displaying horizontal parallel elongations. Framboidal pyrite and celestine crystals are locally abundant.

Crystalline gypsum nodules, coalescing to form parallel enterolitic structures, show a displacive growth deforming the fine-grained

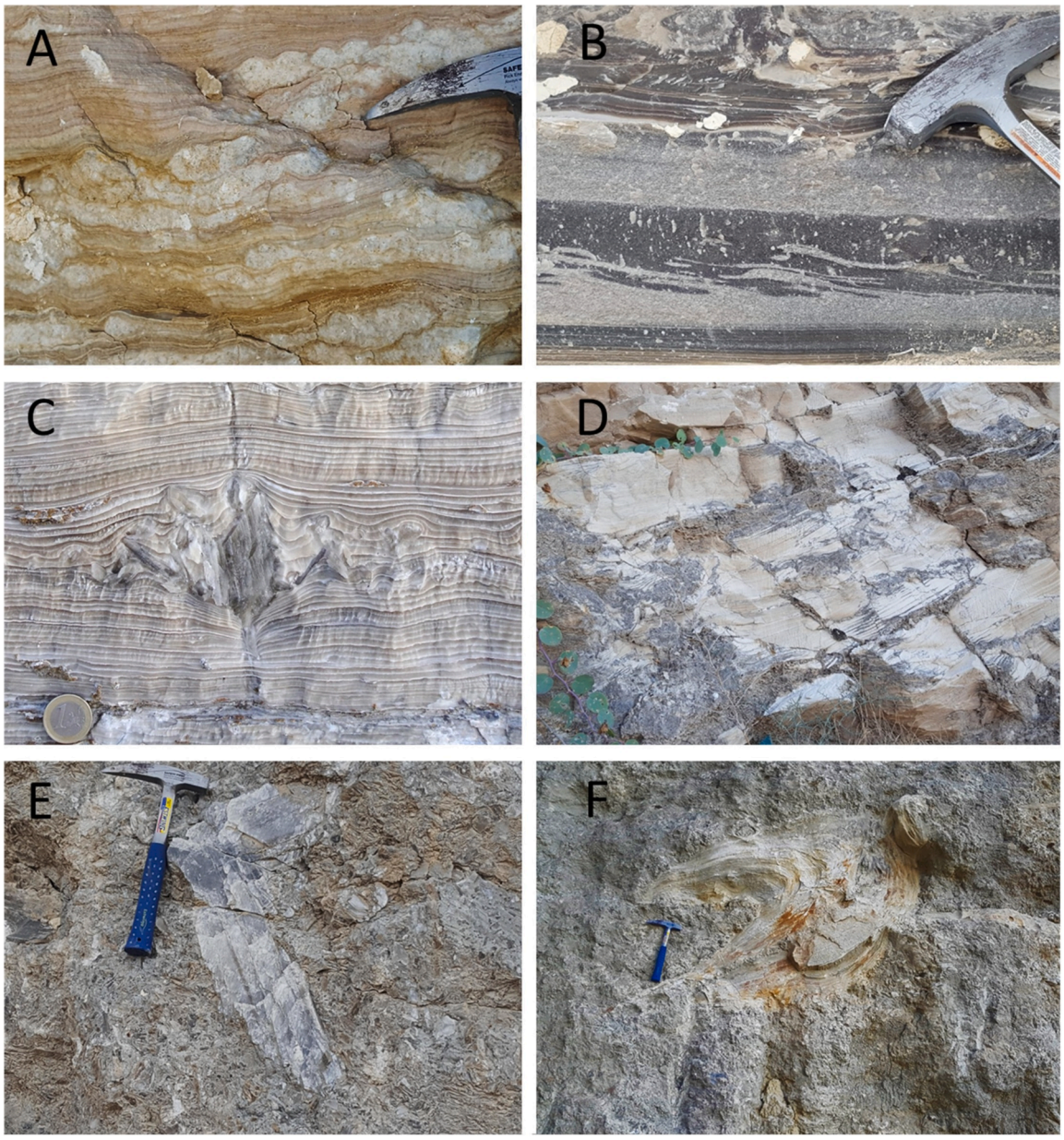

Fig. 4. Gypsum lithofacies. A: Crystalline gypsum nodules deforming lamination (Kalecik); B: Ripple marks and sulfur nodules (Kalecik); C: Selenite clusters within 'in situ' fine-grained laminated gypsum lithofacies; D: Selenite clusters disrupting lamination (Kato Moni); E: Giant twinned selenite clast (Kalecik); F: Deformed fine-grained laminated gypsum clast (Kalecik).

lamination (Fig. 4a). These nodules consist of radial aggregates of prismatic elongated primary gypsum crystals (mm size) without any evidence of anhydrite precursor.

Banded selenite intervals consist of vertically-oriented twinned crystals (cm – dm size) displaying competitive growth. The bottom of each bed generally shows longer crystals. Individual gypsum beds are separated by thin layers of fine-grained gypsum or carbonate laminae (mostly dolomicrite).

Massive selenite beds are equivalent to the "swallow-tail gypsum" term used by Robertson et al. (1995) and to the "non-bedded selenites" of Varol and Atalar (2017). It consists of columns made of twinned gypsum crystals adjacent and stacked one upon another showing a continuous competitive vertical development. Selenite columns growth concurrently, parallel to each other, forming thick selenite beds, more than 0.3 m long (Lugli et al., 2010) and up to 5 m long (giant selenites). Often, the base and top of massive selenite beds contain subhorizontal or randomly oriented crystals. Most selenite crystals show a brownish core with microfilaments resembling the 'spaghetti-like filaments' described in Northern Apennines (Vai and Ricci Lucchi, 1977) and Sicily (Rouchy and Monty, 1999).

Selenite clusters consist of vertically-oriented or non-oriented twinned gypsum crystals (cm-size) growing within fine-grained laminated gypsum and gypsarenite beds (Fig, 4c). They usually show a displacive deformation although locally break the original lamination (Fig. 4d). The lateral growth of several vertically-oriented clusters can coalesce forming selenite layers.

In this work, the terms 'gypsarenite' and 'gypsirudite' are used with genetic connotation in the sense of clastic gypsum deposits resulted from erosion, transport and resedimentation processes.

Gypsarenite beds consist of gypsum crystals with minor carbonate crystals (mainly dolomite), mud and fossils (diatoms and coccoliths) possibly reworked due to the clastic nature of the sediments. Usually, gypsarenites alternate with fine-grained laminated gypsum beds. Parallel laminations, ripples and cross laminations are often recognized

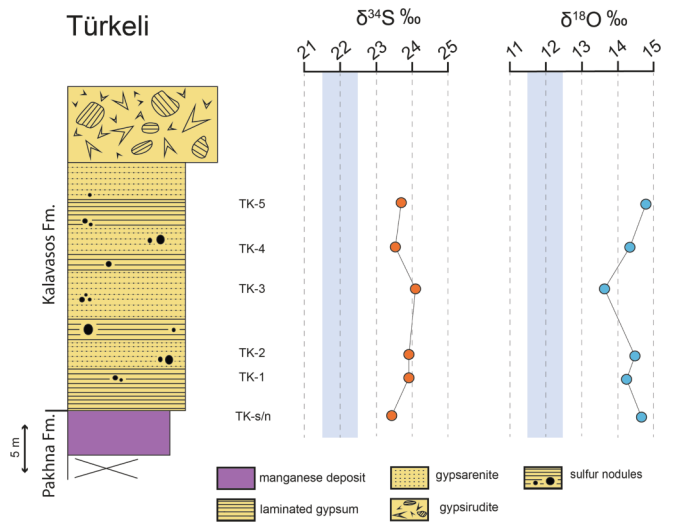

Fig. 5. Türkeli gypsum section. Sulfur and oxygen (in sulfate) isotope profiles. Shaded areas correspond to expected values for Late Miocene marine evaporites (Claypool et al., 1980; Paytan et al., 1998).

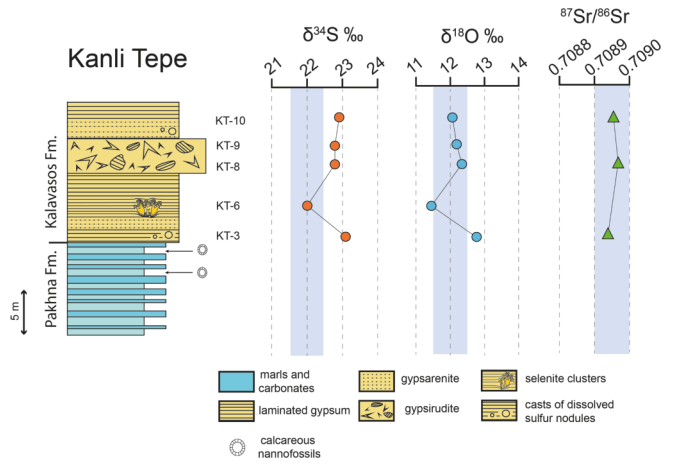

Fig. 6. Kanli Tepe gypsum section. Sulfur, oxygen (in sulfate), and strontium isotope profiles. Shaded areas correspond to expected values for Late Miocene marine evaporites (Claypool et al., 1980; Paytan et al., 1998; Roveri et al., 2014b).

(Fig. 4b).

Gypsirudites show clast-supported fabrics mainly made by broken, abraded or partly dissolved selenite crystals (Fig. 4e). Scattered clasts of fine-grained laminated gypsum, often showing internal soft-sediment deformation, are also frequent (Fig. 4f). Selenite clasts contain 'spaghetti-like' filaments characteristics of the related 'in situ' selenite deposits.

3.2. Mesaoria gypsum successions

Most of the Mesaoria gypsum deposits are buried in the subsurface and therefore not accessible (Gass, 1960; Cleintuar et al., 1977). Outcropping gypsum deposits of the Kalavasos Fm. do not show a complete evaporitic succession. Four stratigraphic sections (Türkeli – *Agios Vesileios*, Kanli Tepe, Akova - *Gypson* and Kalecik - *Gastria*) have been studied in the northern margin of the Mesaoria basin, whereas only one (Kato Moni) in the southern margin. The Kato Moni section corresponds to that previously studied by Pierre (1982) and Manzi et al. (2016). General views, locations, outcrop pictures and primary data (geochemical data and microphotographs) are included as Supplementary Material.

The Türkeli section (Fig. 5) corresponds to one of the westernmost gypsum quarries in the northern margin of the Mesaoria basin (Fig. 2). Hemipelagic marls of the Pakhna Fm., containing a dark purple stratiform manganese deposit (5 m thick), are observed in the base of the quarry. The contact between the Pakhna Fm. and the Kalavasos Fm. is a conformity at the outcrop scale. The gypsum succession is separated in a lower interval (20 m thick) of fine-grained laminated gypsum alternating with gypsarenites, and an upper (7 m thick) gypsirudite interval. Elemental sulfur nodules occur scattered within the lower gypsum interval. $\delta^{34}S_{sulfate}$ and $\delta^{18}O_{sulfate}$ data of the Türkeli gypsum show values of $\delta^{34}S$ ~ 23‰ (23.3–24.1‰) and of $\delta^{18}O$ ~ 14‰ (13.7–14.9‰).

The top of the Pakhna Fm. crops out at the base of the Kanli Tepe quarry, 10 km E of the Türkeli quarry (Fig. 6). These hemipelagic sediments contain abundant calcareous nannoplankton, mainly coccoliths of *Umbilicosphaera Jafari* sp. and *Reticulofenestra minuta sp.*, assemblages of discoaster (Discoaster Broweri group), undifferentiated foraminifera, and fish bone remains. The Kanli Tepe gypsum succession (16 m thick) lie conformably at the outcrop scale upon the Pakhna sediments. Gypsum beds consist of gypsarenites alternating with fine-grained laminated beds. A 3 m thick gypsrudite layer is found 10 m above the Pakhna-Kalavasos boundary. Gypsarenites contain scattered selenite clusters and casts of dissolved sulfur nodules. $\delta^{34}S_{sulfate}$ and $\delta^{18}O_{sulfate}$ data of the Kanli Tepe gypsum beds are ~23‰ (22.0–23.1‰) for $\delta^{34}S$, and of ~12‰ (11.4–12.8‰) for $\delta^{18}O$. Strontium isotope ratios are ~0.7089 (0.70893–0.70896).

The Akova quarry (Fig. 7) shows two banded selenite intervals (12 and 17 m thick) separated by a marl interval (0.5 m thick) containing abundant pyrite framboids, iron oxides, detrital quartz and vegetal remains (Varol and Atalar, 2017). At the top of the quarry, Pliocene sediments of the Nicosia Fm. lay conformably at the outcrop scale over the gypsum succession. $\delta^{34}S_{sulfate}$ and $\delta^{18}O_{sulfate}$ data of the Akova gypsum succession show a narrow range of values, ~ 23‰ (22.6–23.2‰) for $\delta^{34}S$ and ~ 13‰ (12.0–13.4‰) for $\delta^{18}O$. Strontium isotope ratios are ~0.7089 (0.70894–0.70895).

The Kalecik quarry (Fig. 8), 10 km E of the Yeni Iskele village, shows the most complete succession of the Kalavasos Fm. in the Mesaoria basin. Up to 100 m of concordant gypsum beds crop out along two continuous gypsum quarries, one (old quarry) on top of the other (new quarry). The older quarry was previously described by Varol and Atalar (2017). The new quarry, stratigraphically below, has been recently exposed by mining operations. The evaporitic succession, in the new quarry, consists of a 30 m thick interval of gypsirudites and gypsarenites alternating with fine-grained laminated gypsum beds. Enterolitic layers of crystalline radiating gypsum and sulfur nodules occur in the lowermost part. A fine-grained laminated gypsum bed, 5 m thick, is recognized in both the top of the new quarry and at the base of the older quarry. The old quarry shows the uppermost 70 m of the evaporite succession and consists of a lower mixed (laminated to disoriented and vertically-oriented selenites) gypsum bed followed by six vertically-oriented selenite beds (between 7 and 15 m thick) of banded and massive lithofacies, separated by fine-grained gypsum intervals (between 0.5 and 1 m thick). Pliocene marine sediments rest conformably, at the outcrop scale, over the gypsum beds of the old quarry. $\delta^{34}S_{sulfate}$ and $\delta^{18}O_{sulfate}$ data of the Kalecik gypsum beds show $\delta^{34}S$ values ~23‰ (22.6–23.6‰). However, the $\delta^{18}O$ profile can be divided in two different parts. The lower part, characterized by clastic gypsum beds, shows $\delta^{18}O$ values ~12‰ (11.8–13.7‰) while, the upper part, represented by vertically-oriented selenites, has values of ~13‰ (12.6–13.5‰). Strontium isotope ratios in the Kalecik gypsum do not show differences between the new and old quarries, with values ~0.7089 (0.70894–0.70896).

The Kato Moni gypsum succession (Fig. 9), on the southern margin of the Mesaoria basin (Fig. 2), consists of 4 banded selenite intervals (3–5 m thick) separated by fine-grained laminated gypsum levels (1–2 m thick). $\delta^{34}S_{sulfate}$ and $\delta^{18}O_{sulfate}$ data of Kato Moni gypsum are ~23‰

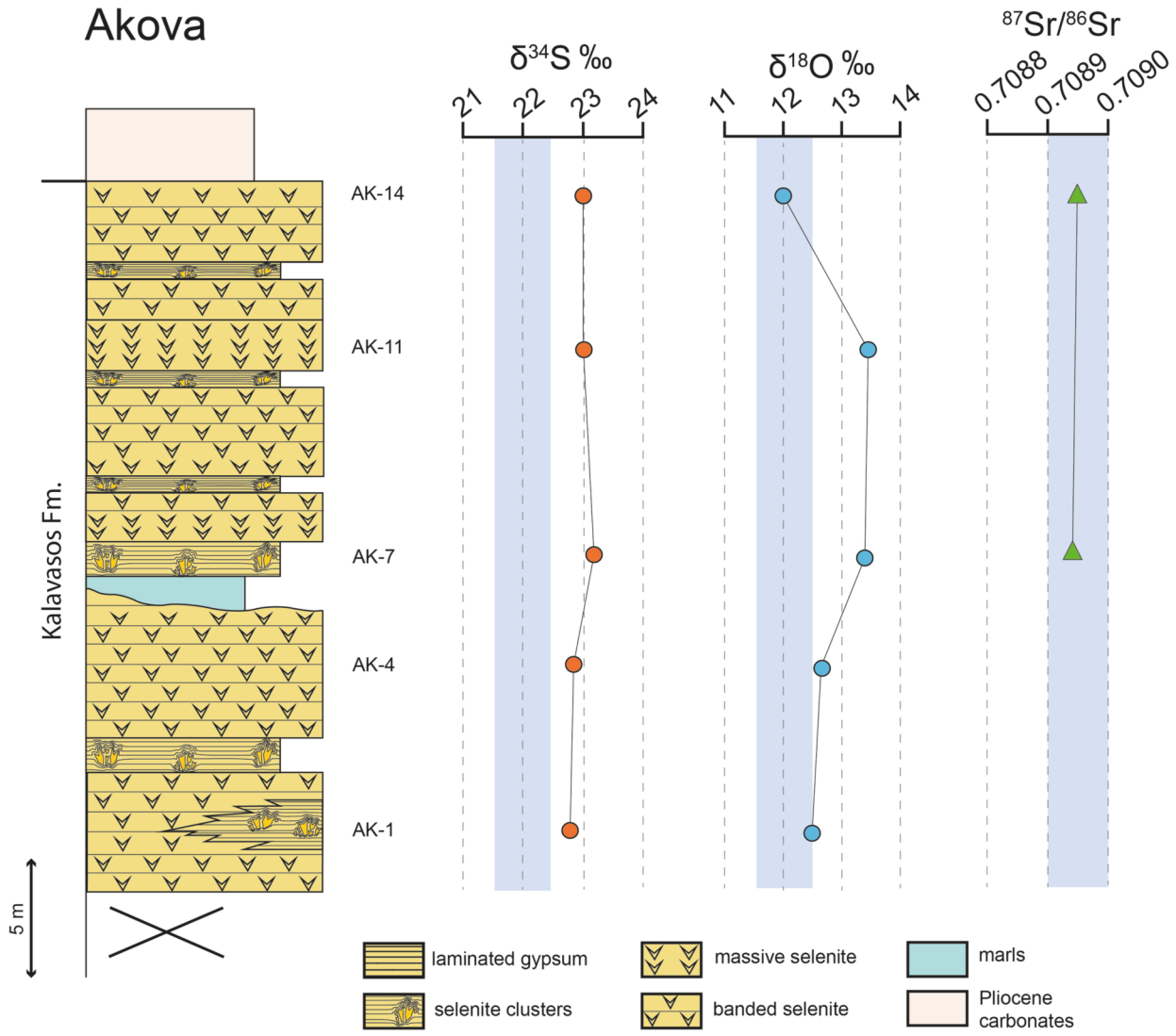

Fig. 7. Akova gypsum section. Sulfur, oxygen (in sulfate), and strontium isotope profiles. Shaded areas correspond to expected values for Late Miocene marine evaporites (Claypool et al., 1980; Paytan et al., 1998; Roveri et al., 2014b).

(22.9–23.3‰) for $\delta^{34}S$, and ~ 13‰ (12.5–14.0‰) for $\delta^{18}O$. Strontium isotope ratios are ~0.7089.

4. Discussion

4.1. North Cyprus MSC evaporites: Genetic and stratigraphic relationships

In North Cyprus, the Messinian evaporites of the Kalavasos Fm. largely consist of 'in situ' gypsum beds precipitated/grown in the place where they are found, and clastic gypsum beds transported and resedimented away from where originally precipitated.

Fine-grained laminated gypsum can correspond both to 'in situ' or to clastic facies. As 'in situ' facies, fine-grained gypsum crystals nucleate from a sulfate oversaturated brine, falling and accumulating on the basin floor (Garber et al., 1987; Krumgalz, 2019). As resedimented facies, fine-grained gypsum crystals can be transported towards deeper sites. Fine-grained 'balatino' gypsum deposits in the Northern Apennines, previously interpreted as deep-water primary gypsum deposits, are now considered clastic deposits formed by gravitational flows (Manzi et al., 2005). In the absence of other clastic evidence (detritic clasts, cross-bedding, ripple marks, etc.) we interpret fine-grained gypsum beds as 'in situ' cumulate deposits when intercalate between bottom-grown vertically-oriented selenite beds, and as clastic deposits when intercalate between gypsarenites and gypsirudites.

Gypsarenites and gypsirudites of the Kalavasos Fm. in North Cyprus are interpreted as gravity-flow gypsum deposits. These clastic gypsum deposits derived from the erosion and resedimentation of vertically-oriented selenite gypsum deposits previously formed on shallower marginal surrounding areas (Fig. 10). Instabilities in the marginal selenite platforms, tectonic and/or eustatic in origin, led to the erosion of marginal selenite deposits resedimented basinward as gravity-flow gypsum deposits (Fig. 10).

Crystalline gypsum enterolites (Fig. 4a) show displacive-growth within clastic fine-grained deposits, whereas vertically-oriented selenite cluster appears within 'in situ' fine-grained laminated gypsum deposits (Fig. 4c). Both lithofacies are interpreted as early diagenetic interstitial growths within unconsolidated gypsum sediments. Locally unoriented gypsum clusters formed filling fractures in poorly cemented gypsum beds (Fig. 4d).

A correlation chart of the North Cyprus Kalavasos Fm. is proposed in Fig. 11. A bed-to-bed correlation has not been possible because the long distance between outcrops and the absence of key beds. The North Cyprus MSC gypsum succession is subdivided in two different units. The lower unit, best represented in westward sections (Türkeli, Kanli Tepe), mainly consists of clastic gypsum facies, whereas the upper unit, well

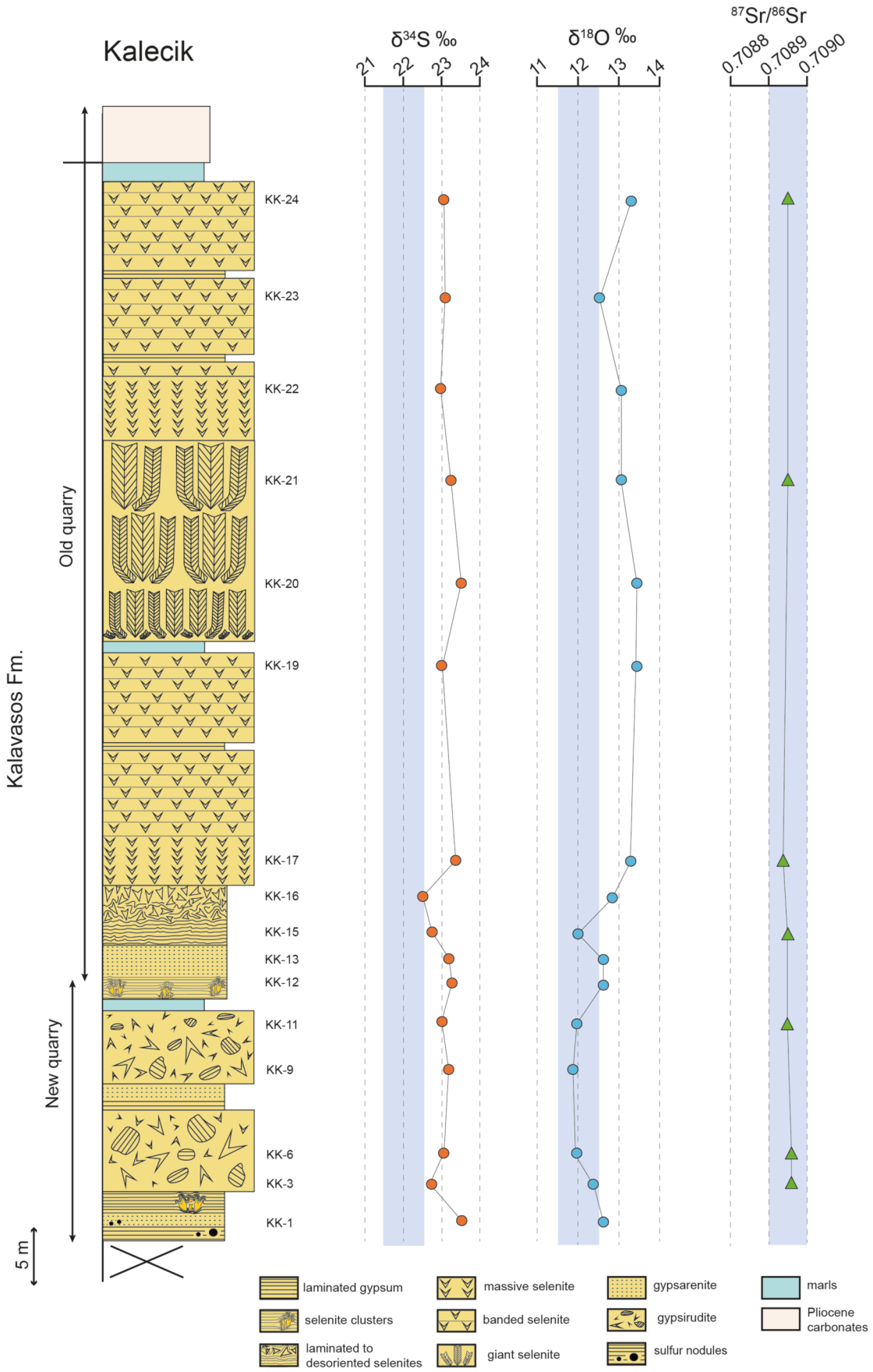

Fig. 8. Kalecik gypsum section. Sulfur, oxygen (in sulfate), and strontium isotope profiles. Shaded areas correspond to expected values for Late Miocene marine evaporites (Claypool et al., 1980; Paytan et al., 1998; Roveri et al., 2014b).

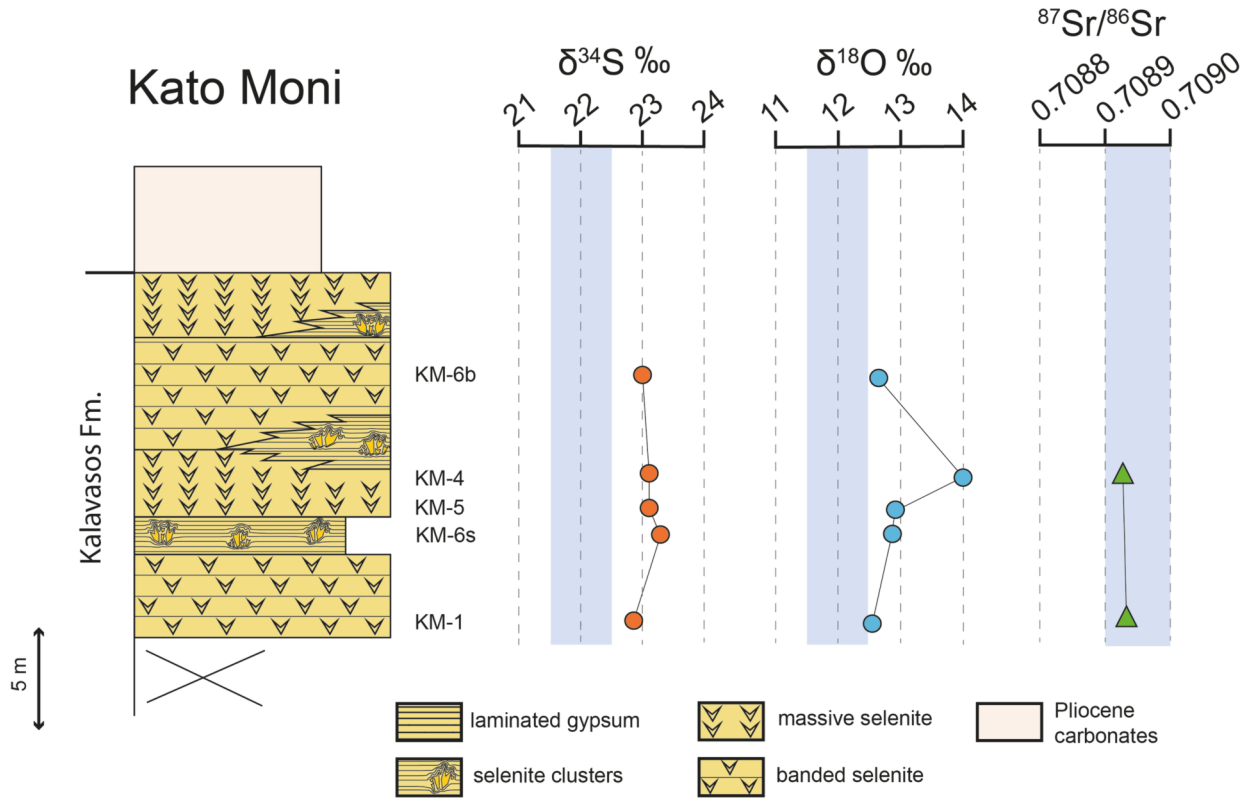

Fig. 9. Kato Moni gypsum succession. Sulfur, oxygen (in sulfate), and strontium isotope profiles. Shaded areas correspond to expected values for Late Miocene marine evaporites (Claypool et al., 1980; Paytan et al., 1998; Roveri et al., 2014b).

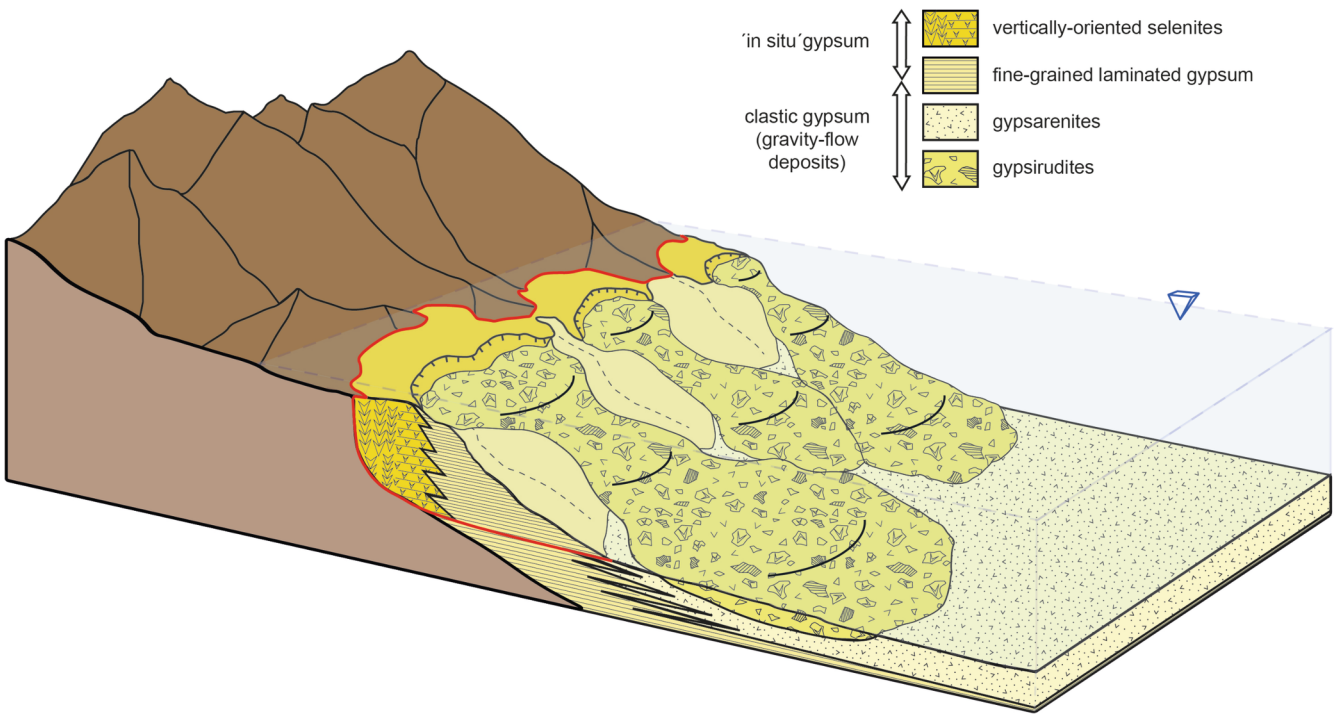

Fig. 10. Depositional model for MSC gyspsum deposists of the Kalavasos Fm. in the North Cyprus Mesaoria basin.

preserved in the eastward sections (Kato Moni, Akova, Kalecik) mainly consists of 'in situ' vertically-oriented selenite facies. Both parts are well exposed in the Kalecik section.

The stratigraphic succession in North Cyprus, with deeper clastic gypsum deposits followed upwards by 'in situ' selenite platforms represents a shallowing regressive trend (Fig. 12). Selenite platforms, initially formed in marginal areas, were eroded during the relative sea-level drop and resedimented as gravity-flow gypsum deposits in deeper

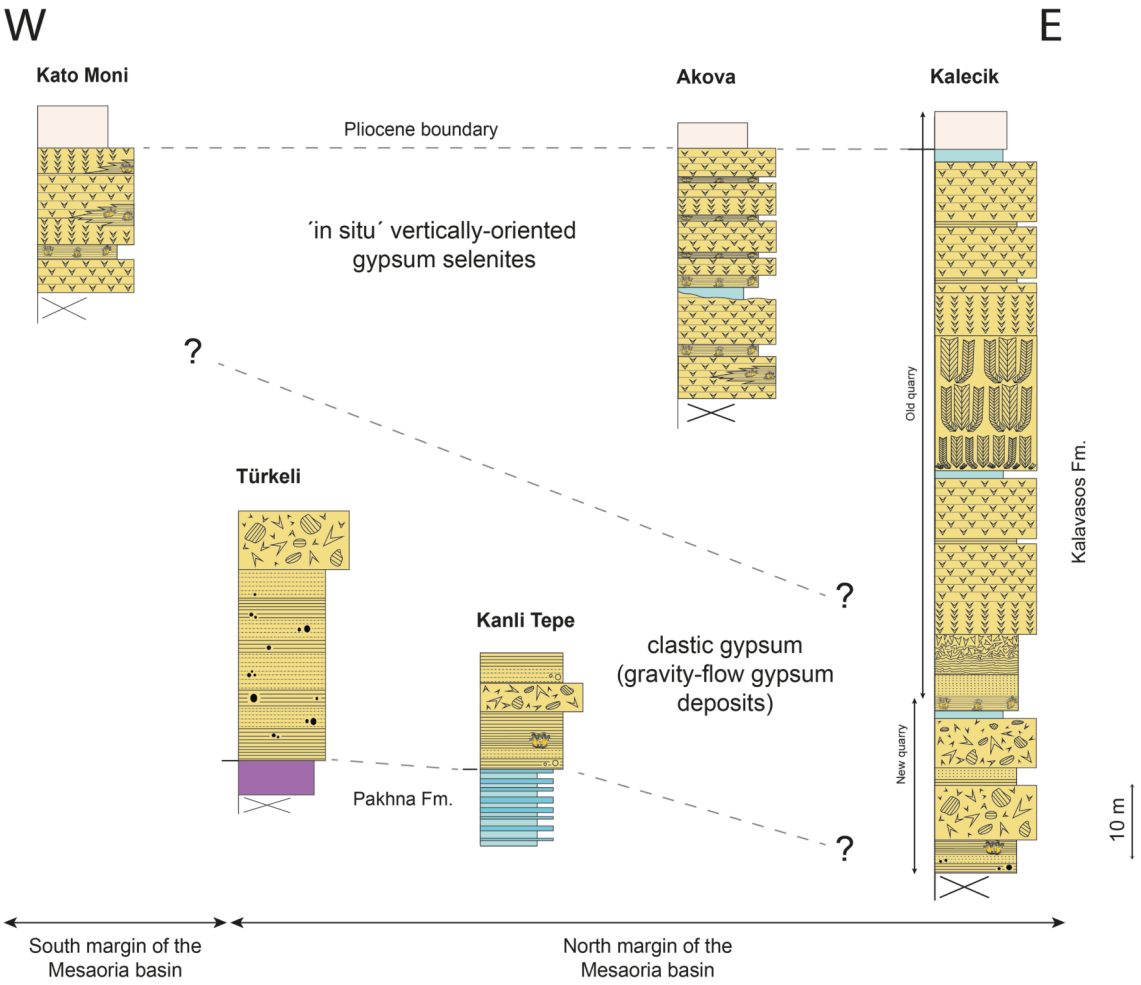

Fig. 11. Correlation chart of MSC gypsum sections of the Kalavasos Fm. in the Mesaoria basin (North Cyprus).

areas. As the sea level continued to drop, the staked clastic lobes were subsequently overlaid by younger selenite platforms.

4.2. Geochemical signatures in the Mesaoria evaporites

Isotopic gypsum data in the North Cyprus Kalavasos Fm. are very homogeneous and do not show significant differences between the stratigraphic lower (gravity-flow gypsum deposits) and upper (selenite platform deposits) units. Isotope compositions in gypsum sulfate are of $\delta^{34}S \sim 23‰$ (22.0–24.1‰) and of $\delta^{18}O \sim 13‰$ (11.4–14.9‰). North Cyprus MSC evaporites reflect relative isotopic enrichments of ~1‰ for $\delta^{34}S$, and of ~1–2‰ for $\delta^{18}O$ compared with expected for Late Miocene marine evaporites ($\delta^{34}S \sim 22‰$ and $\delta^{18}O \sim 12‰$). Similar enrichments have been reported for the Lower Evaporites (PLG and RLG units in the 'three-stage' model) in different Western Mediterranean basins: Sorbas, Bajo Segura and Mallorca basins (Spain), Caltanissetta (Sicily), and in the Eastern Mediterranean Polemi basin (South Cyprus) (García-Veigas et al., 2018 and references therein).

Strontium isotope ratios in North Cyprus evaporites (~ 0.7089) are in range with those reported for Lower Evaporites (PLG and RLG deposits in the 'three-stage' model) (Roveri et al., 2014b, and references therein).

According to sulfur, oxygen (in sulfate), and strontium isotope data, we interpret that the entire evaporite succession in North Cyprus (Mesaoria basin) corresponds to the MSC Lower Evaporites in the classical 'two-step' lithostratigraphic division. In our opinion, differentiation between PLG and RLG is isotopically questionable because RLG deposits are, in origin, evaporites precipitated during MSC stage 1 and then resedimented during MSC stage 2 (Roveri et al., 2008b, 2014a). No isotopic fractionation occurs during gypsum resedimentation so, gypsum deposits of both stages should keep the same sulfate and strontium isotope signatures.

4.3. Discrepancies with the gypsum lithostratigraphic framework proposed by Roveri et al. (2014a)

MSC clastic gypsum deposits assigned to the RLG (MSC stage 2) in the Roveri et al. (2014a) model are recognized either in western (Sicily and North Apennines) and eastern (Greece and South Cyprus) Mediterranean. In this chronostratigraphic model, RLG (MSC stage 2) deposits post-date the 'in situ' vertically-oriented selenite sequences of the PLG (MSC stage 1) unit. According to this model, the main phase of the erosion (MES) entirely follows the deposition of the PLG. This phase is linked to the subaerial exposure of the basin margins following the deterioration of the Atlantic-Mediterranean exchange and the consequent drop of the Mediterranean base-level. However, RLG deposits are never found laterally or vertically in continuity with PLG deposits. Where both PLG and RLG deposits are recognized in the same basin, they are always separated by faults, thrust fronts or other structural elements as occurs in the Northern Apennines (Manzi et al., 2007) or North Sicily (Roveri et al., 2008a).

Unlike the widespread distribution in many MSC Mediterranean basins of 'Lago Mare' deposits assigned to the MSC stage 3 in the Roveri et al. (2014a) model (Andreetto et al., 2021, for a review), outcropping Upper Evaporites – UG (MSC stage 3) deposits are only limited to Siciliy (Decima and Wezel, 1971; Rouchy, 1982; Roveri et al., 2006; Roveri

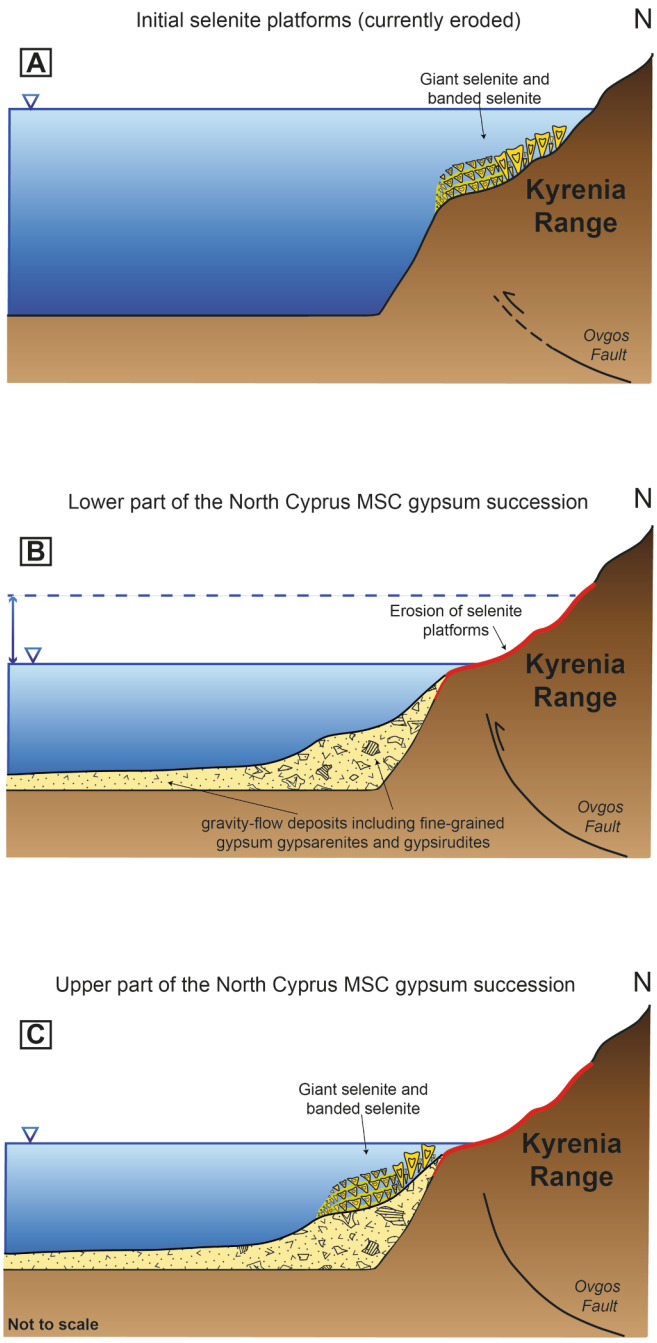

Fig. 12. Evolutive model for the gypsum succession of the Kalavasos Fm. in the Mesaoria basin (North Cyprus).

et al., 2008a, 2008c; Manzi et al., 2009; Caruso et al., 2015) and South Cyprus (Rouchy and Pierre, 1979; Rouchy, 1982; Pierre, 1982; Manzi et al., 2016).

In the North Cyprus Mesaoria basin, the lower unit of the Kalavasos Fm. consists of clastic gypsum similar to those reported for RLG units in Northern Apennines (Manzi et al., 2007) and South Cyprus (Manzi et al., 2016), whereas the upper unit shows vertically-oriented selenite gypsum lithofacies characteristic of both PLG and UG units.

Tentatively, following the 'three-stage' model of Roveri et al. (2014a), the lower part of the North Cyprus gypsum succession could be assigned to the RLG unit, and the upper to the UG unit. However, the upper part does not show the characteristic stacking pattern (gypsum – marl cycles) and does not contain Lago Mare flora and fauna typical of the UG deposits in Sicily and South Cyprus (Rouchy et al., 2001; Manzi et al., 2009, 2016; Roveri et al., 2014a). Furthermore, our geochemical data show that the upper part is consistent with isotopic values found in other vertically-oriented selenite deposits assigned to the PLG deposits. The PLG assignation of the upper part, conformably overlying clastic gypsum tentatively assigned to RLG deposits, conflicts with the gypsum lithostratigraphic succession proposed in the Roveri et al. (2014a) model.

Based on lithostratigraphic and isotopic data, we assign the complete gypsum succession of the Kalavasos Fm. in North Cyprus to the MSC Lower Evaporites in the sense of the classical stratigraphic division (Lower and Upper Evaporites) summarized and outlined in Rouchy and Caruso (2006). The Roveri et al. (2014a) chronostratigraphic model, mainly based on Sicily, cannot be applied to the North Cyprus Messinian evaporites.

Our assignation implies that, at least in North Cyprus, vertically-oriented selenite platforms tentatively assigned to the PLG in the Roveri et al. (2014a) model underwent erosion coevally with its formation. Selenite platforms, eroded and resedimented, and subsequently overlaid by younger selenite platforms must be considered within the same MSC chronostratigraphic unit.

4.4. *MSC evaporites in North and South Cyprus*

In South Cyprus, three gypsum lithostratigraphic units are recognized in the Messinian Kalavasos Fm.: Lower Gypsum, Intermediate Gypsum Breccia, and Upper Gypsum (Rouchy, 1982; Pierre, 1982; Robertson et al., 1995; Rouchy et al., 2001; Orszag-Sperber et al., 2009). In these works, assignation of each gypsum unit to the classic MSC stratigraphic division (Lower Evaporites and Upper Evaporites) is suggested rather than concluded. Rouchy et al. (2001) identify Lago Mare fauna assemblages, similar to those reported from other Mediterranean basins (Andreetto et al., 2021, for a review), in the latest intergypsum intervals and in the post-evaporitic deposits.

Recently, Manzi et al. (2016) recognize a clastic origin for most gypsum beds of the Lower Gypsum in South Cyprus, identify the Messinian Erosional Surface at its base, and propose the assignation of the Lower Gypsum and the Intermediate Gypsum Breccia units to the RLG deposits (MSC stage 2) in the Roveri et al. (2014a) model. Based on lithological features and strontium isotope ratios, these authors assign the selenite-bearing Upper Gypsum unit of Rouchy (1982) to the UG unit (MSC stage 3) in the Roveri et al. (2014a) model.

In North Cyprus, the work of Manzi et al. (2016) is limited to the study of the Kato Moni section (Fig. 9), in the southern margin of the Mesaoria basin (Fig. 2). Based on gypsum lithofacies and on an interpreted stratigraphic unconformity assigned to the Messinian Erosional Surface (MES), they suggest that this small gypsum outcrop belongs to the UG unit (MSC stage 3). We disagree because the Kato Moni gypsum succession does not show the marked marl-gypsum cyclicity characteristic of the UG deposits (Manzi et al., 2009; Roveri et al., 2014a), there are not $^{87}Sr/^{86}Sr$ isotope data and/or Lago Mare records supporting this assignation and lastly, the interpreted erosional surface probably corresponds to a tectonic control.

Some lithological similitudes, but important geochemical differences, exist between the gypsum successions assigned to the different MSC units/ stages in South (Polemi, Pissouri, and Maroni basins) and North (Mesaoria basin) Cyprus. The lower part of the evaporite succession, in both North and South Cyprus, is characterized by clastic gypsum deposits with sulfate and strontium isotope signatures in range with other MSC Lower Evaporites. However, important differences exist in the upper part of each evaporite succession. In South Cyprus, the upper part shows facies associations and isotope data similar to those reported for Upper Evaporites – UG (MSC stage 3) deposits in Sicily. However, in North Cyprus, the upper part is characterized by facies association, and isotope signatures in range with Lower Evaporites – PLG and RLG (MSC stages 1 and 2).

Manzi et al. (2016) propose a North Cyprus – South Cyprus

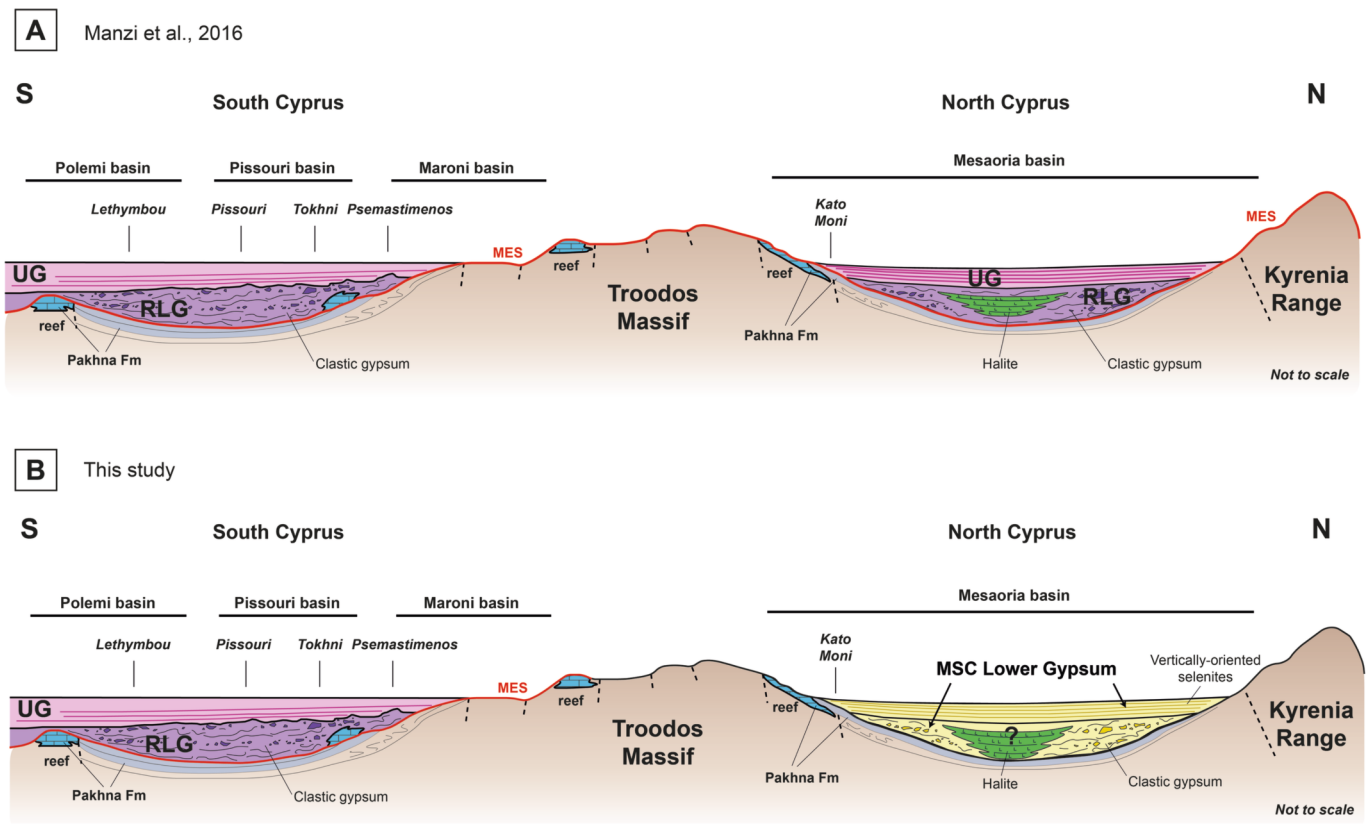

Fig. 13. Schematic geological section of MSC gypsum deposits (Kalavasos Fm.) in South and North Cyprus. A: Manzi et al. (2016); B: This work.

geological correlation of the MSC evaporites (Fig. 13). Although their observation is only limited to the Kato Moni gypsum quarry in North Cyprus, where clastic gypsum deposits do not crop out, they recognize extensive RLG and UG units in both parts of the island. We propose a new correlation chart (Fig. 13) in which Lower and Upper Evaporite deposits, in the sense of the classical MSC stratigraphic division, are represented in South Cyprus, and only Lower Evaporite deposits in North Cyprus.

5. Conclusions

Despite the current use of the unifying three-stage litho- and chronostratigraphic frame (PLG, RLG, and UG) proposed by Roveri et al. (2014a) to different MSC gypsum deposits across the Mediterranean, marked differences exists between the MSC gypsum successions recorded in South (Polemi, Pissouri and Psemastimenos basins) and North (Mesaoria basin) Cyprus.

Correlative sections in the northern margin of the Mesaoria basin divide the North Cyprus MSC gypsum succession in two gypsum units. Following the Roveri et al. (2014a) model, the lower unit, mainly consisting of clastic gravity-flow gypsum deposits, could be tentatively assigned to RLG deposits (MSC stage 2). Whereas, the upper part, characterized by 'in situ' vertically-oriented selenite beds, should be assigned to PLG deposits (MSC stage 1).

The complete Kalavasos Fm., in North Cyprus, is characterized by homogeneous sulfur and oxygen (in sulfate) isotope compositions ($\delta^{34}S$ ~ 23‰ and $\delta^{18}O$ ~ 13‰) and strontium isotope ratios ($^{87}Sr/^{86}Sr$ ~ 0.7089). These values match those reported for MSC Lower Evaporites in the classic 'two-step' model (Rouchy and Caruso, 2006, for a review) that integrate PLG (MSC stage 1) and RLG (MSC stage 2) deposits in the 'three-stage' model of Roveri et al. (2014a). Unlike in South Cyprus, Upper Evaporites - Upper Gypsum (MSC stage 3) deposits are absent in the North Cyprus Mesaoria basin.

The evaporite succession in North Cyprus, with clastic gravity-flow gypsum deposits overlaid by 'in situ' selenite gypsum platforms, both geochemically assigned to MSC Lower Evaporites in the classical lithostratigraphic division, raised concerns to the extension of the currently accepted 'three-stage' model to other MSC Mediterranean basins where local tectonics, bathymetric and paleogeographic factors could led to different gypsum facies distributions.

Declaration of Competing Interest

The authors declare that they have no known competing financial interests or personal relationships that could have appeared to influence the work reported in this paper.

Acknowledgments

This study was provided by the Spanish Government Projects CGL-2016-79458 and PID2020-118999GB-I00, and by the Catalonian Government Action 21-SGR-829. The authors are indebted to Francesca Lozar for her help in nannofossil identification, to Rosa Maria Marimón and Eva Aracil (Universitat de Barcelona) for their technical support in isotope spectrometry, and to Antonio Caruso, an anonymous reviewer and the editor for their insightful reviews and contributions.

Appendix A. Supplementary data

Supplementary data to this article can be found online at https://doi.org/10.1016/j.palaeo.2021.110681.

References

Andreetto, F., Aloisi, G., Raad, F., Heida, H., Flecker, R., Agiadi, K., Lofi, J., Blondel, S., Bulian, F., Camerlenghi, A., Caruso, A., Ebner, R., Garcia-Castellanos, D., Gaullier, V., Guibourdenche, L., Gvirtzman, Z., Hoyle, T.M., Meijer, P.T.,

Moneron, J., Sierro, F.J., Travan, G., Tzevahirtzian, A., Vasiliev, I., Krijgsman, W., 2021. Freshening of the Mediterranean Salt Giant: controversies and certainties around the terminal (Upper Gypsum and Lago-Mare) phases of the Messinian Salinity Crisis. Earth-Sci. Rev. 216, 103577.
Babel, M., 2007. Depositional environments of a saline-type evaporite basin recorded in the Badenian gypsum facies in the northern Carpathian Foredeep. Geochem. Soc. Spec. Publ. 285, 107–142.
Butler, R.W.H., Lickorish, W.H., Grasso, M., Pedley, H.M., Ramberti, L., 1995. Tectonics and sequence stratigraphy in Messinian basins, Sicily: constraints on the initiation and termination of the Mediterranean salinity crisis. Geol. Soc. Am. Bull. 107, 425–439.
Caruso, A., Pierre, C., Blanc-Valleron, M.M., Rouchy, J.M., 2015. Carbonate deposition and diagenesis in evaporitic environments: the evaporative and Sulphur-bearing limestones during the settlement of the Messinian salinity crisis in Sicily and Calabria. Paleogeogr. Palaeoclimatol. Palaeoecol. 429, 136–162.
CIESM, 2008. The Messinian salinity crisis from mega-deposits to microbiology. A consensus report. In: Briand, F. (Ed.), CIESM Workshop Monographs, 33, 96 pp.
Cita, M.B., Wright, R.C., Ryan, W.B.F., Longinelli, A., 1978. Messinian paleoenvironments. In: Hsü, et al. (Eds.), Initial Reports of the Deep Sea Drilling Project 42A. USA Government Printing Office, Washington DC, pp. 1003–1035.
Clauzon, G., Suc, J.P., Gautier, F., Berger, A., Loutre, M.F., 1996. Alternate interpretation of the Messinian salinity crisis: controversy resolved? Geology 24, 363–366.
Claypool, G.E., Holser, W.T., Kaplan, I.R., Sakai, H., Zak, I., 1980. The age curves of sulfur and oxygen isotopes in marine sulfate and their mutual interpretation. Chem. Geol. 28, 199–260.
Cleintuar, M.R., Knox, G.J., Ealey, P.J., 1977. The geology of Cyprus and its place in the East-Mediterranean framework. Geol. Mijnb. 56, 66–82.
Decima, A., Wezel, F.C., 1971. Osservazioni sulle evaporiti messiniane della Sicilia centro-meridionale. Rivista Mineraria Siciliana 22, 171–187 (in Italian).
Flecker, R., Ellam, R.M., 2006. Identifying late Miocene episodes of connection and isolation in the Mediterranean-Paratethyan reals using Sr isotopes. Sediment. Geol. 188–189, 189–203.
Flecker, R., de Villiers, S., Ellam, R.M., 2002. Modelling the effect of evaporation on the salinity–87Sr/86Sr relationship in modern and ancient marginal-marine systems: the Mediterranean Messinian Salinity Crisis. Earth Planet. Sci. Lett. 203, 221–233.
Fortuin, A.R., Krijgsman, 2003. The Messinian of the Nijar basin (SE Spain): sedimentation, depositional environments and paleogeographic evolution. Sediment. Geol. 160, 213–242.
Garber, R.A., Levy, Y., Friedman, G.M., 1987. The sedimentology of the Dead Sea. Carbponates and Evaporites 2, 43–53.
García-Veigas, J., Cendón, D.I., Gibert, L., Lowenstein, T.K., Artiaga, D., 2018. Geochemical indicators in Western Mediterranean Messinian evaporites: implications for the salinity crisis. Mar. Geol. 403, 197–214.
Gass, T.M., 1960. The geology and mineral resources of the Dhali area. Geol. Survey Depart. Cyprus Memoir 4, 116 pp.
Gass, I.G., Cockbain, A.E., 1961. Notes on the occurrence of gypsum in Cyprus. Overseas Geol. Min Res. 8, 279–287.
Guerra-Merchán, A., Serrano, F., Hlila, R., El Kadiri, K., de Galdeano, C.S., Garcés, M., 2014. Tectono-sedimentary evolution of the peripheral basins of the Alboran Sea in the arc of Gibraltar during the latest Messinian-Pliocene. J. Geodyn. 77, 158–170.
Hsü, K.J., Ryan, W.B.F., Cita, M.B., 1973. The Miocene desiccation of the Mediterranean. Nature 242, 240–244.
Hsü, K.J., Montadert, L., Bernoulii, D., Cita, M.B., Erickson, A., Garrison, R.E., Kidd, R.B., Mélières, F., Müller, C., Wright, R., 1977. History of the Mediterranean salinity crisis. Nature 267, 1053–1078.
Kampschulte, A., Strauss, H., 2004. The sulfur isotopic evolution of Phanerozoic seawater based on the analysis of structurally substituted sulfate in carbonates. Chem. Geol. 204, 255–286.
Kasprzyk, A., 1997. Oxygen and Sulphur isotope composition of Badenian (Middle Miocene) gypsum deposits in southern Poland: a preliminary study. Geol. Quart. 41, 53–60.
Kinnaird, T.C., 2008. Tectonic and sedimentary response to oblique and incipient continental-continental collision the easternmost Mediterranean (Cyprus). PhD Thesis. University of Edinburgh, 380 pp.
Kinnaird, T.C., Robertson, A.H.F., 2012. Tectonic and sedimentary response to subduction and incipient continental collision in southern Cyprus, easternmost Mediterranean region. Geol. Soc. Lond. Spec. Publ. 372, 585–614.
Kinnaird, T.C., Robertson, A.H.F., Morris, A., 2011. Timing of uplift of the Troodos Massif (Cyprus) constrained by sedimentary and magnetic polarity evidence. J. Geol. Soc. 168, 457–470.
Krabbenhöft, A., Eisenhauer, A., Böhm, F., Vollstaedt, H., Fietzke, J., Liebetrau, V., Augustin, N., Peucker-Ehrenbrink, B., Müller, M.N., Horn, C., Hansen, B.T., Nolte, N., Wallmann, K., 2010. Constraining the marine strontium budget with natural strontium isotope fractionations ($^{87}Sr/^{86}Sr$, $\delta^{88/86}Sr$) of carbonates, hydrothermal solutions and river waters. Geochim. Cosmochim. Acta 74, 4097–4109.
Krijgsman, W., Hilgen, F.J., Marabini, S., Vai, G.B., 1999. Chronology, causes and progression of the Messinian salinity crisis. Nature 400, 652–655.
Krijgsman, W., Blanc-Valleron, M.M., Flecker, R., Hilgen, F.J., Kouwenhoven, T.J., Orszag-Sperber, F., Rouchy, J.M., 2002. The onset of the Messinian salinity crisis in the eastern Mediterranean (Pissouri Basin, Cyprus). Earth Planet. Sci. Lett. 194, 299–310.
Krumgalz, B., 2019. On the problem of gypsum deposition in the Dead Sea in the case of two seas canal construction. Am. J. Chem. Phys. Chem. 8, 58–65.
Lofi, J., Gorini, Ch., Berné, S., Clauzon, G., Tadeus Dos Reis, A., Ryan, W.B.F., Steckler, M.S., 2005. Erosional processes and paleo-environmental changes in the Western Gulf of Lions (SW France) during the Messinian salinity crisis. Mar. Geol. 217, 1–30.
Lu, F.H., Meyers, W.J., 2003. Sr, Sc, and OSO4 isotopes and the depositional environments of the Upper Miocene evaporites, Spain. J. Sediment. Res. 73, 444–450.
Lu, F.H., Meyers, W.J., Schoonen, M.A., 2001. S and O (SO_4) isotopes, simultaneous modeling, and environmental significance of the Nijar messinian gypsum, Spain. Geochim. Cosmochim. Acta 656, 3081–3092.
Lugli, S., Manzi, V., Roveri, M., Schreiber, B.Ch., 2010. The primary lower gypsum in the Mediterranean: A new facies interpretation for the first stage of the Messinian salinity crisis. Palaeogeogr. Palaeoclimatol. Palaeoecol. 297, 83–99.
Manzi, V., Lugli, S., Lucchi, F.R., Roveri, M., 2005. Deep-water clastic evaporites deposition in the Messinian Adriatic foredeep (northern Apennines, Italy): did the Mediterranean ever dry out? Sedimentology 52, 875–902.
Manzi, V., Roveri, M., Gennari, R., Bertini, A., Biffi, U., Giunta, S., Iaccarino, S.M., Lanci, L., Lugli, S., Negri, A., Riva, A., Rossi, M.E., Taviani, M., 2007. The Deep-water counterpart of the Messinian lower Evaporites in the Apennine foredeep. Palaeogeogr. Palaeoclimatol. Palaeoecol. 251, 470–499.
Manzi, V., Lugli, S., Roveri, M., Schreiber, B.C., 2009. A new facies model for the Upper Gypsum of Sicily (Italy): chronological and paleoenvironmental constraints for Messinian salinity crisis in the Mediterranean. Sedimentology 56, 1937–1960.
Manzi, V., Gennari, R., Hilgen, F., Krijgsman, W., Lugli, S., Roveri, M., Sierro, F.J., 2013. Age refinement of the Messinian salinity crisis onset in the Mediterranean. Terra Nova 0, 1–8.
Manzi, V., Lugli, S., Roveri, M., Dela Pierre, F., Gennari, R., Lozar, F., Natalicchio, M., Schreiber, B.Ch., Taviani, M., Turco, E., 2016. The Messinian salinity crisis in Cyprus: a further step towards a new stratigraphic framework for Eastern Mediterranean. Basin Res. 28, 159–297.
McCay, G.A., 2011. Tectonic-sedimentary evolution of the (Kyrenia) Girne Range and the Mesarya (Meraoria) Basin, North Cyprus. PhD Thesis. University of Edinburgh, 586 pp.
McCay, G.A., Robertson, A.H.F., 2013. Upper Miocene–Pleistocene deformation of the Girne (Kyrenia) Rangeand Dar Dere (Ovgos) lineaments, northern Cyprus: role in collision and tectonic escape in the easternmost Mediterranean region. Geol. Soc. Lond. Spec. Publ. 372, 421–445.
Müller, D.W., Mueller, P.A., 1991. Origin and age of the Mediterranean Messinian evaporites: implications from Sr isotopes. Earth Planet. Sci. Lett. 107, 1–12.
Necdet, M., Anıl, M., 2006. The geology and geochemistry of the gypsum deposits in Northern Cyprus. Geosound 48, 11–49.
Ogniben, L., 1957. Petrografia della serie solfifera-siciliana e considerazioni geotechniche relative. Memorie descrittive della carta Geologica d'Italia 33, 1–275 (in Italian).
Orszag-sperber, F., Caruso, A., Blanc-valleron, M.M., Merle, D., Rouchy, J.M., 2009. The onset of the Messinian salinity crisis: insights from Cyprus sections. Sediment. Geol. 217, 52–64.
Palamakumbura, R.N., Robertson, A.H.F., 2016. Pleistocene terrace formation related to surface tectonic up-lift: example of the Kyrenia Range lineament in the northern part of Cyprus. Sediment. Geol. 339, 46–67.
Palmer, M.R., Edmond, J.M., 1992. Controls over the strontium isotope composition of river water. Geochim. Cosmochim. Acta 56, 2099–2111.
Pantazis, T.M., 1976. Thermal mineral waters of Cyprus. In: Proceedings International Congress on thermal Waters, Geothermal energy and Volcanism, Mediterranean area, Vol. 2, pp. 367–386. Athens.
Papadimitriou, N., Gorini, C., Nader, F.H., Deschamps, R., Symeou, V., Lecomte, J.C., 2018. Tectono-stratigraphic evolution of the western margin of the Levant Basin (offshore Cyprus). Mar. Pet. Geol. 91, 683–705.
Paytan, A., Kastner, M., Campbell, D., Thiemens, M.H., 1998. Sulfur isotopic composition of Cenozoic seawater sulfate. Science 282, 1459–1462.
Pearce, C.R., Parkinson, I.J., Gaillardet, J., Charlier, B.L.A., Mokadem, F., Burton, K.W., 2015. Reassing the stable ($\delta^{88/86}Sr$) and radiogenic ($^{87}Sr/^{86}Sr$) strontium isotopic composition of marine inputs. Geochemica et Cosmochimica Acta 157, 125–146.
Pierre, C., 1982. Teneurs en isotopes stables (^{18}O, ^{13}C, ^{2}H, ^{34}S) et conditions de genèse des évaporites marines: application à quelques milieux actuels et au Messinien de la Méditerranée. PhD Thesis. Universite de Paris-Sud Centre d'Orsay. in French.
Reinhardt, E.G., Stanley, D.J., Patterson, R.T., 1998. Strontium isotopic- paleontological method as a high-resolution paleosalinity tool for lagonal environments. Geology 26, 1003–1006.
Robertson, A.H.F., Hudson, J.D., 1974. Pelagic sediments in the cretaceous and Tertiary history of the Troodos Massif, Cyprus, 1. International Association of Sedimentology Special Publications, pp. 403–436.
Robertson, A.H.F., Kinnaird, T.C., 2016. Structural development of the Central Kyrenia Range (North Cyprus) in its regional setting in the eastern Mediterranean region. Int. J. Earth Sci. 105, 417–437.
Robertson, A.H.F., Eaton, S., Follows, E.J., Payne, A.S., 1995. Depositional processes and basin analysis of Messinian evaporites in Cyprus. Terra Nova 7, 233–253.
Robertson, A.H.F., Necdet, M., Raffi, I., Chen, G., 2019. Early Messinian manganese deposition in NE Cyprus related to cyclical redox changes in a silled hemipelagic basin prior to the Mediterranean salinity crisis. Sediment. Geol. 385, 126–148.
Rouchy, J.M., 1982. La genèse des évaporites messiniennes de Méditerranée. PhD Thesis. Mémoires du Muséum d'Histoire Naturelle, Paris. in French.
Rouchy, J.M., Caruso, A., 2006. The Messinian salinity crisis in the Mediterranean basins: a reassessment of the data and integrated scenario. Sediment. Geol. 188–189, 35–67.
Rouchy, J.M., Monty, C.L.V., 1999. Microbial gypsum sediments: Neogene and Modern examples. In: Riding, R., Awramik, S.M. (Eds.), Microbial Sediments. Springer-Verlag, pp. 209–216.

Rouchy, J.M., Pierre, C., 1979. Données sédimentologiques et isotopiques sur les gypses des séries évaporitiques messiniennes d'Espagne meiridionale et de Chypre. Reveu de géographuie physique et de géologie dynamique 21, 267–280.
Rouchy, J.M., Taberner, C., Peryt, T.M., 2001. Sedimentary and diagenetic transitions between carbonates and evaporites. Sediment. Geol. 140, 1–8.
Rouchy, J.M., Caruso, A., Pierre, C., Blanc-Valleron, M.M., Bassetti, M.A., 2007. The end of the Messinian salinity crisis: evidences from the Chelif Basin (Algeria). Palaeogeogr. Palaeoclimatol. Palaeoecol. 254, 386–417.
Roveri, M., Manzi, V., 2006. The Messinian salinity crisis: looking for a new paradygm? Palaeogeogr. Palaeoclimatol. Palaeoecol. 238, 386–398.
Roveri, M., Lugli, S., Manzi, V., Schreiber, B.C., Caruso, A., Rouchy, J.M., Iaccarino, S.M., Gennari, R., Vitale, F.P., 2006. Clastic vs. primary precipitated evaporites in the Messinian Sicilian basins. In: RCMNS Interim colloquium (Parma), Post-Congress Field-Trip, 66 pp.
Roveri, M., Lugli, S., Manzi, V., Gennari, R., 2008a. Large-scale mass wasting processes in the Messinian Ciminna Basin (northern Sicily). GeoActa 7, 81–98.
Roveri, M., Lugli, S., Manzi, V., Schreiber, B.C., 2008b. The Messinian Sicilian stratigraphy revisited: toward a new scenario for the Messinian salinity crisis. Terra Nova 20, 483–488.
Roveri, M., Lugli, S., Manzi, V., Schreiber, B.C., 2008c. The Messinian salinity crisis: a sequence-stratigraphic approach. GeoActa Spec. Publicat. 1, 169–190.
Roveri, M., Flecker, R., Krijgsman, W., Lofi, J., Lugli, S., Manzi, V., Sierro, F., Bertini, A., Camerlenghi, A., De Lange, G., Govers, R., Hilgen, F., Hübscher, C., Meijer, P.T., Stoica, M., 2014a. The Messinian salinity crisis: past and future of a great challenge for marine sciences. Mar. Geol. 352, 25–58.
Roveri, M., Lugli, S., Manzi, V., Gennari, R., Schreiber, B.C., 2014b. High-resolution strontium isotope stratigraphy of the Messinian deep Mediterranean basins: implications for marginal to central basin correlation. Mar. Geol. 349, 113–125.
Ryan, W.B.F., 1976. Quantitative evaluation of the depth of the western Mediterranean before, during and after the late Miocene salinity crisis. Sedimentology 23, 791–813.
Sampalmieri, G., Cipollari, P., Cosentino, D., Iadanza, A., Lugli, S., Soligo, M., 2008. Le facies evaporitiche della crisi di salinità messiniana: radioattività naturalle. Boll. Soc. Geol. Ital. 127, 25–36.
Samplamieri, G., Iadanza, A., Cipollari, P., Cosentino, D., Lo Mastro, S., 2010. Paleoenvironments of the Mediterranean Basin at the Messinian hypersaline/hyposaline transition: evidence from natural radioactivity and microfacies of post-evaporitic successions of the Adriatic sub-basin. Terra Nova 22, 239–250.
Selly, R., 1973. An outline of the Italian Messinian. In: Drooger, C.W. (Ed.), Messinian Events in the Mediterranean. North Holland Publishing Company, Amsterdam, Netherlands, pp. 150–171.
Topper, R.P.M., Flecker, R., Meijer, P.T., Wortel, M.J.R., 2011. A box model of the late Miocene Mediterranean Sea: implications from combined 87Sr/86Sr and salinity data. Paleoceanography 26.
Turchyn, A.V., Schrag, D.P., 2004. Oxygen isotope constraints on the sulfur cycle over the past 10 million years. Science 303, 2004–2007.
Vai, G.B., Ricci Lucchi, F., 1977. Algal crusts, autochtonous and clastic gypsum in a cannibalistic evaporite basin; a case history from the Messinian of Northern Apennine. Sedimentology 24, 211–244.
Varol, B., Atalar, C., 2017. Messinian evaporites in the Mesaoria Basin, North Cyprus: facies and environmental interpretations. Carbonates Evaporites 32, 349–365.
Zomenis, S.L., 1972. Stratigraphy and hydrogeology of the Neogene rocks in the northern foothills of the Troodos Massif. Cyprus. Bull. Geol. Surv. Depart. Cyprus 5, 22–90.